RSC Advances

PAPER

View Article Online
View Journal | View Issue

Cite this: *RSC Adv.*, 2020, **10**, 26467

Cu(II) immobilized on Fe_3O_4@HNTs–tetrazole (CFHT) nanocomposite: synthesis, characterization, investigation of its catalytic role for the 1,3 dipolar cycloaddition reaction, and antibacterial activity†

Zoleikha Hajizadeh, Fereshte Hassanzadeh-Afruzi, Diana Fallah Jelodar, Mohammad Reza Ahghari and Ali Maleki *

Received 30th May 2020
Accepted 2nd July 2020

DOI: 10.1039/d0ra04772d

rsc.li/rsc-advances

In the present study, Cu(II) immobilized on an Fe_3O_4@HNTs–tetrazole (CFHT) nanocomposite was designed and prepared. For this, halloysite nanotubes (HNTs) as natural mesoporous substances were modified during several chemical reactions. The synthesis of the CFHT nanocomposite was investigated step by step with the required physicochemical techniques such as FT-IR, EDX, SEM, TEM, XRD, VSM, TGA and CHNS analyses. After ensuring that the nanocomposite was successfully prepared, its catalytic application in the synthesis of the 5-substituted 1*H*-tetrazole derivatives *via* multicomponent reactions (MCRs) between aromatic aldehydes, malononitrile, and sodium azide was assessed. According to the experimental results, the prepared nanocomposite exhibited excellent capability for conducting this MCR reaction. All desired products were obtained in a short reaction time (30–40 min) with high productivity (90–97%) and without a complicated workup procedure. Furthermore, the magnetic property of the synthesized heterogeneous nanocomposite empowers it to be recovered and reused in five times successive reactions without any significant reduction in reaction efficiency. Moreover, the remarkable antibacterial activity of the nanocomposite against *Escherichia coli* (*E. coli*) and *Staphylococcus aureus* (*S. aureus*) was evaluated by agar diffusion and plate-count methods. The zones of inhibition were around 16 and 20 mm for *E. coli* and *S. aureus* bacteria, respectively. Also, colony analysis confirms the killing of bacteria by using the CFHT nanocomposite.

1. Introduction

Nanotubes have been a novel and fast-growing field of nanotechnology in recent research. The properties of organic or inorganic nanotubes can be altered by functionalizing the surface of these materials by covalent or non-covalent interactions.[1] Halloysite is a natural aluminosilicate clay with a nanotube structure that possesses positive and negative charges on the inner and outer surfaces. The presence of negative and positive charges is associated with the existence of silicate and alumina groups in this material.[2] HNTs are known as mesoporous compounds with an average outer diameter and an inner diameter of about 50 nm and 12 nm, respectively. Under acidic, alkaline or thermal conditions, the size of the porous of HNTs could be altered.[3] HNTs, with interesting features such as biocompatibility, chemical modification, high water uptake, and affordability are widely employed in diverse fields such as biomedical, tissue engineering, absorbents, and cosmetics.[4–7] The existence of a great deal of hydroxyls as active functional groups on the inner and outer walls of HNTs permits them to be chemically modified. In recent years, the modification of HNTs by magnetic nanoparticles has been frequently reported in the scientific literature.[8–10] The modified nanocomposites have been utilized in some areas such as reduction of nitrophenol, dyes removal.[11,12] The metals-containing nanocatalysts with their applicable properties have been mostly employed to assist diverse chemical reactions, such as oxidation and reduction reactions, coupling, cross-coupling, multicomponent reactions, click and cycloaddition reactions under the convenient and benign procedure. Copper is one of those intermediate metals that has gained much attention with appreciated features such as availability, biocompatibility, affordable price, catalytic efficiency for some reactions and its outstanding antimicrobial activity against various bacterial strains.[11] Several hybrid composites have recently been fabricated by immobilizing copper on the organic, inorganic or hybrid compounds and then utilized as efficient catalytic or antibacterial systems.[12–16] MCRs are one-pot methods in which simple initial materials incorporated into the direct manufacture of complex structures.[17,18] Atomic economy, high efficiency, convergence, high bond-forming index are such outstanding features of MCRs. Therefore, the synthesis of many complicated heterocycles compound, intricate pharmaceutical molecules, and natural

Catalysts and Organic Synthesis Research Laboratory, Department of Chemistry, Iran University of Science and Technology, Tehran 16846-13114, Iran. E-mail: maleki@iust.ac.ir; Fax: +98-21-73021584; Tel: +98-21-73228313

† Electronic supplementary information (ESI) available: ^{1}H and ^{13}C NMR spectra. See DOI: 10.1039/d0ra04772d

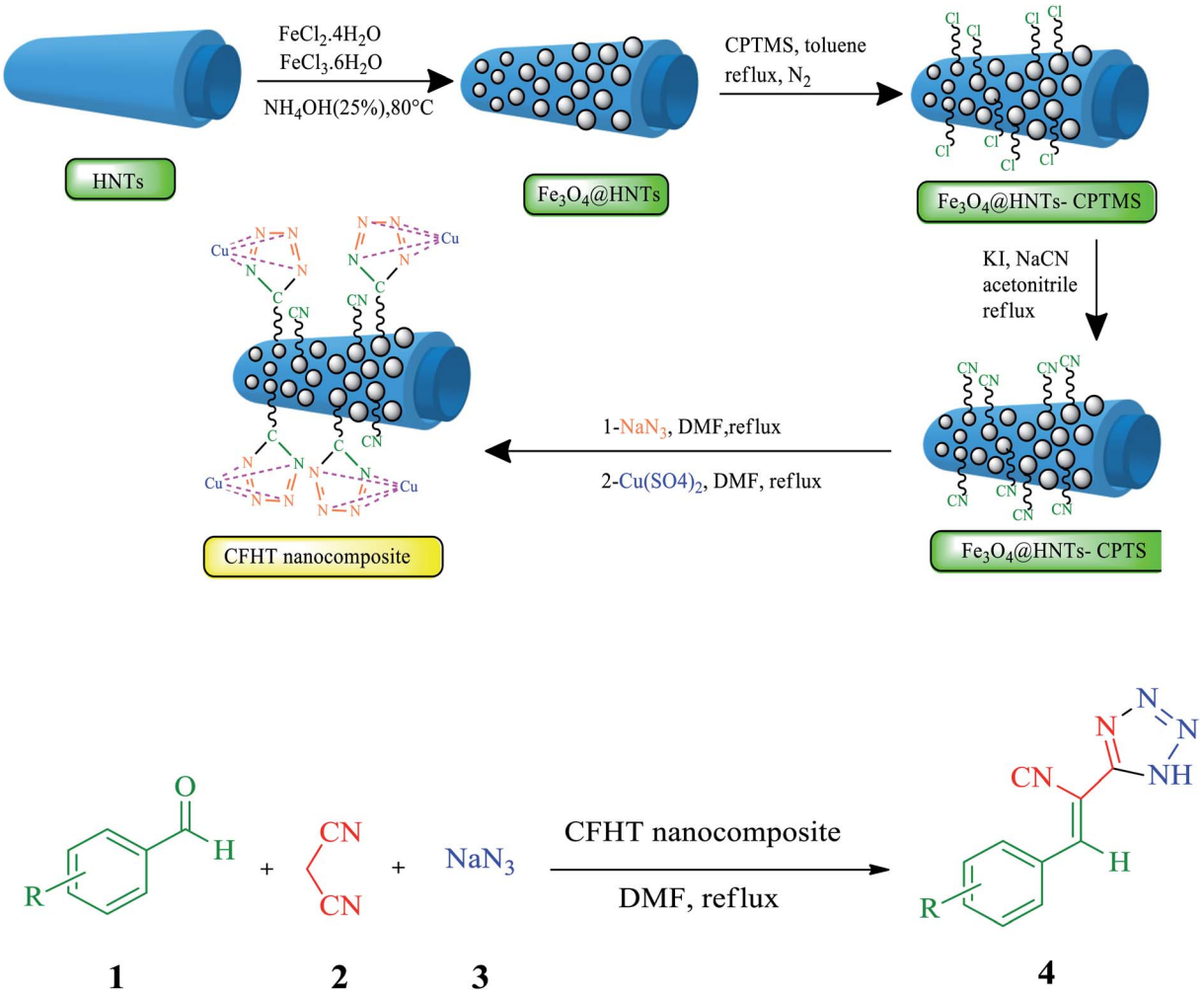

Fig. 1 The preparation pathway of the CFHT nanocomposite and production of 5-substituted 1*H*-tetrazoles derivatives.

products are accomplished using these kinds of reactions.[19–21] Tetrazoles and their derivatives are an important member of N-containing heterocycles family which potential application in coordination chemistry, material science, organometallic chemistry, pharmacology, imaging materials, and military.[22] The close acidity of this functional group and the carboxylic group resulted in their application as potential pharmaceutical material and the preparation of some compounds such as losartan, irbesartan, tomelukast, and PTZ (2). 5-Substituted tetrazoles also possess biological and pharmacological activities, such as antimicrobial, antidiabetic, antiviral and antihypertensive and have potential therapeutic effects against cerebral ischemia and schizophrenia. They are potential antibacterial and antifungal activities and have shown variable growth inhibitory effects on Gram-positive and Gram-negative bacteria. Some researches focused on the evaluation of these compounds suitability for antibiotics and their cytotoxicity.[23–25] The synthesis of tetrazoles has been developed by various methods and diverse catalysts due to the importance of these compounds as one of the main constituents of organic compounds and their biological and pharmaceutical properties. Although most of the reported methods offered advantages, there are still some issues such as unapproachability or toxicity of reagents, non-recyclable catalysts, unproductive efficiency and long reaction times.

In this study, CFHT nanocomposite was introduced as an effectiveness heterogeneous nanocatalyst in connection with our recent research on the design and development of natural material based hybrid catalysts. This heterogeneous nanocatalyst was designed, prepared by several step chemical reactions, characterized successfully and its catalytic application was assessed for speeding up the synthesis of 5-substituted 1*H*-tetrazoles derivatives. The CFHT nanocomposite preparation pathway and production of 5-substituted 1*H*-tetrazoles derivatives *via* MCRs between aromatic aldehydes (**1**), malononitrile (**2**) and sodium azide (**3**) have been schematically illustrated in Fig. 1.

2. Result and discussion

The catalyst synthesis process involves several steps as follows:

(1) Preparation of the Fe_3O_4@HNTs through simple chemical precipitation of HNTs and two kinds of iron chloride salts in alkaline condition.

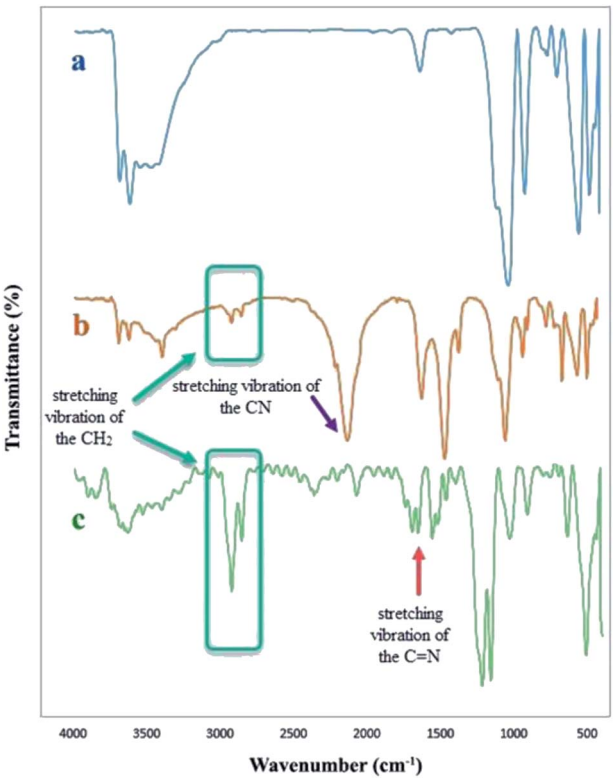

Fig. 2 The FT-IR spectra of the Fe_3O_4@HNTs (a), Fe_3O_4@HNTs–CPTS (b) and CFHT nanocomposite (c).

(2) Surface modification of the Fe_3O_4@HNTs with (3-chloropropyl)triethoxysilane (CPTMS) to prepare Fe_3O_4@HNTs–CPTMS.

(3) The reaction of the Fe_3O_4@HNTs–CPTMS with NaCN to produce the Fe_3O_4@HNTs–CPTS nanocomposite.

(4) The preparation of Fe_3O_4@HNTs–tetrazole through the 1,3 dipolar cycloaddition reaction between the Fe_3O_4@HNTs–CPTS and NaN_3.

(5) And the final step was immobilization of Cu(II) onto the Fe_3O_4@HNTs–tetrazole by using an aqueous solution of $Cu(SO_4)_2$ to obtain CFHT nanocomposite.

2.1. Characterization of the CFHT nanocomposite

Various physicochemical identification analyses have employed to study the structural and distinctive characteristics of the synthesized catalysts (CFHT nanocomposite), and the results are delicately discussed.

2.1.1. FT-IR spectroscopy. FT-IR spectroscopy was used to investigate the step-by-step construction of catalysts and approve the presence of expected functional groups. The spectra of Fe_3O_4@HNTs (a), Fe_3O_4@HNTs–CPTS (b) and CFHT nanocomposite (c) were presented in Fig. 2. As mentioned earlier, the HNTs are natural aluminosilicate, therefore in the IR spectrum of Fe_3O_4@HNTs (a), the stretching and bending vibrations of the Si–O–Si, Al–O–Al, Al–O–Si bonds, the hydroxyl functional groups and the Fe–O bonds of Fe_3O_4 should be observed. Thus, in the Fe_3O_4@HNTs (a), spectrum, there are the absorption bands at 466 and 540 cm^{-1} (the bending vibration of Si–O–Si and Al–O–Si), 690, 756 and 1022 cm^{-1} (the stretching vibrations of Si–O–Si), 910 cm^{-1} (the bending vibration of Al–O–H). Also, the absorptions at 3618 cm^{-1} and 3687 cm^{-1} (the stretching vibrations of OH bonds of the inner-surface of Al–OH). Stretching vibration of Fe–O and OH bond of Fe_3O_4 overlapped with the bending vibrations of Al–O–Si and OH bonds of the inner-surface of Al–OH.[8,9] The (b)

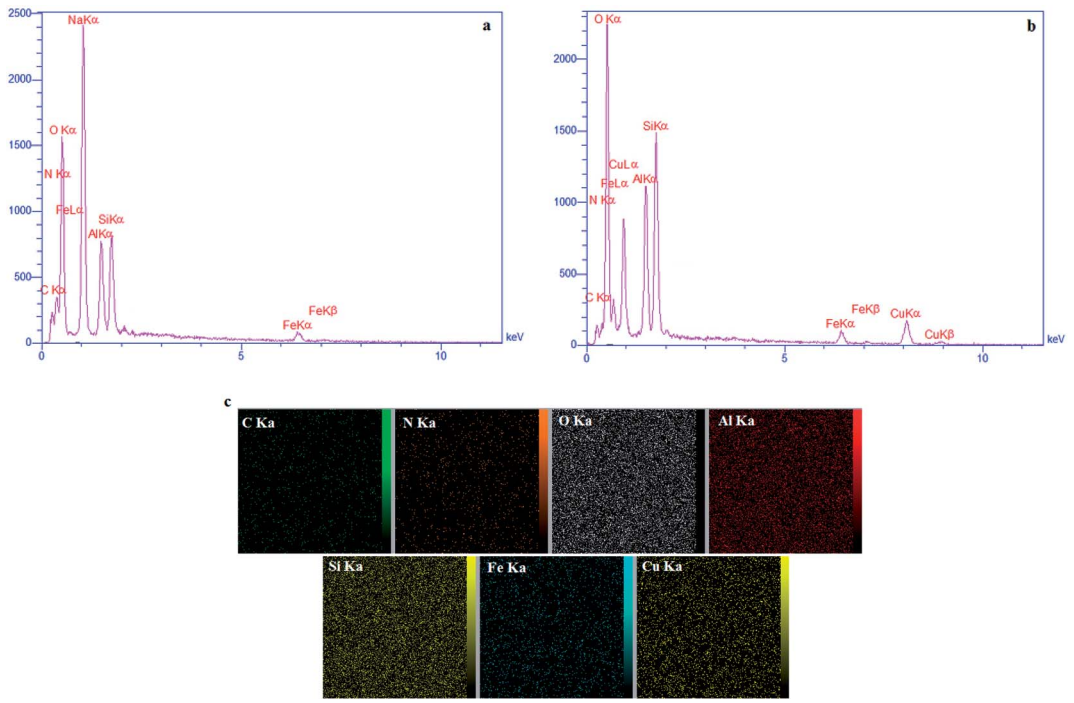

Fig. 3 EDX analysis of the Fe_3O_4@HNTs–CPTS (a), the CFHT nanocomposite (b) and mapping images of the CFHT nanocomposite (c).

Table 1 The result of elemental analysis (CHNS)

Sample	% C	% H	% N
Fe_3O_4@HNTs–CPTS	3.09	1.53	2.35
Fe_3O_4@HNTs–tetrazole	6.29	1.54	16.69

spectrum belongs to the Fe_3O_4@HNTs–CPTS. As clearly observed, in addition to the absorptions in the Fe_3O_4@HNTs, strong adsorption at 2117 cm^{-1} coming from the stretching vibration of the CN functional group, and two adsorptions at 2850 and 2916 cm^{-1} ascribed to aliphatic CH_2 stretching vibrations.

As expected, several new bands become apparent at 2117, 2850 and 2916 cm^{-1} that were corresponded to the stretching vibrations of the CN functional group and aliphatic CH_2 bond, respectively, approval of surfaces chemical modification of the Fe_3O_4@HNTs with the (3-cyanopropyl)triethoxysilane (CPTS). The FT-IR of CFHT nanocomposite was observed in the spectrum (c). This nanocomposite was the result of two steps reaction of the Fe_3O_4@HNTs–CPTS. The first one was the click reaction with sodium azide to create Fe_3O_4@HNTs–tetrazole composite and the next one was the coordination of Cu(II) onto the tetrazole ring of Fe_3O_4@HNTs–tetrazole. What was expected to be observed is that the strong absorption at 2117 cm^{-1} that existed in the spectrum (b) (signifying the presence of the nitrile group) must be either eliminated or reduced in intensity. As seen in the spectrum (c), that absorption was disappeared. In addition, a new absorption band appeared in 1652 cm^{-1} is related to the stretching vibration of the C=N bond in the tetrazole ring of the CFHT nanocomposite approving the construction of this nanocomposite.

2.1.2. EDX analysis. EDX analysis was conducted to determine the elements in the prepared samples qualitatively. For the Fe_3O_4@HNTs–CPTS, the results of this analysis displayed the presence of iron, oxygen and nitrogen elements which could be acceptable evidence of the modification of the Fe_3O_4@HNTs surface by the CPTS. The EDX and mapping images of CFHT nanocomposite, in addition to the elements in the preceding sample, showed a new intensive peak for the copper element. Therefore, it can be inferred that the copper was loaded onto the tetrazole ring of Fe_3O_4@HNTs–tetrazole (Fig. 3).

2.1.3. CHNS analysis. Following an IR and EDX analyses, the construction of the Fe_3O_4@HNTs–CPTS and Fe_3O_4@HNTs–tetrazole composite was further investigated by CHNS analysis. The percentages of C, N and H elements for these two samples are presented in Table 1. A comparison of the percentages of N in the two samples showed that the percentage of nitrogen increased from 2.35% in the Fe_3O_4@HNTs–CPTS to 16.69% in the Fe_3O_4@HNTs–tetrazole nanocomposite. In other words, the ratio of nitrogen to carbon in the Fe_3O_4@HNTs–tetrazole is 3.48 times that of the Fe_3O_4@HNTs–CPTS.

2.1.4. SEM analysis. SEM analysis was employed to find out the shape, morphology, particle distribution, and even the average particle size of the CFHT nanocomposite. SEM images showed two kinds of morphologies in the resulting nanocomposite. Some nanotube particles encircled by many spherical particles. The average particle size of these spherical particles is approximately 26 nm with a uniform particle size distribution. Given that the nanotube morphology has been

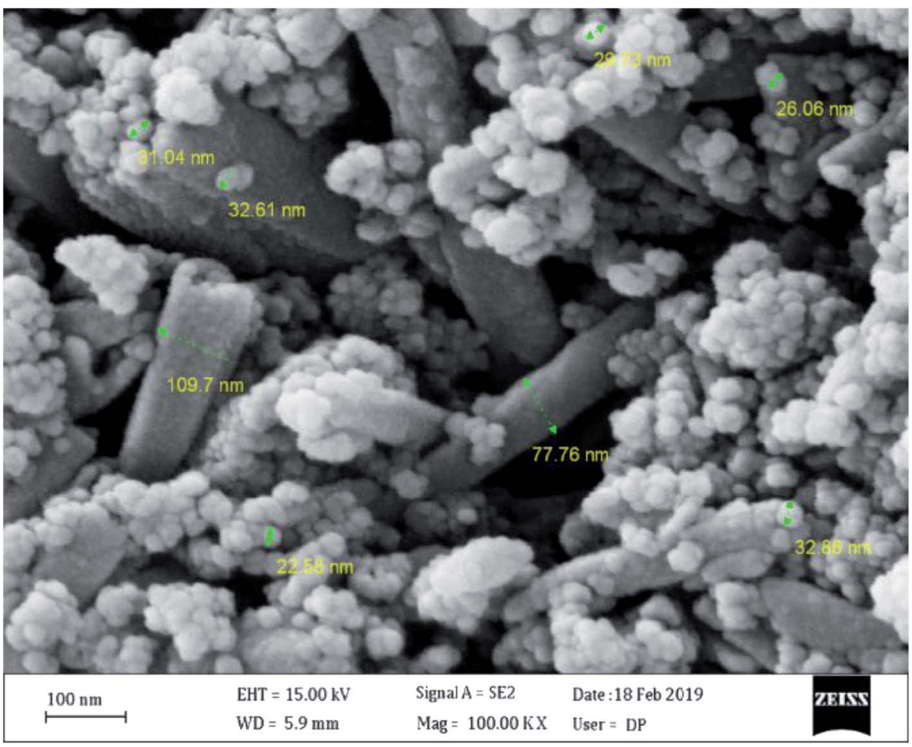

Fig. 4 SEM images of the CFHT nanocomposite.

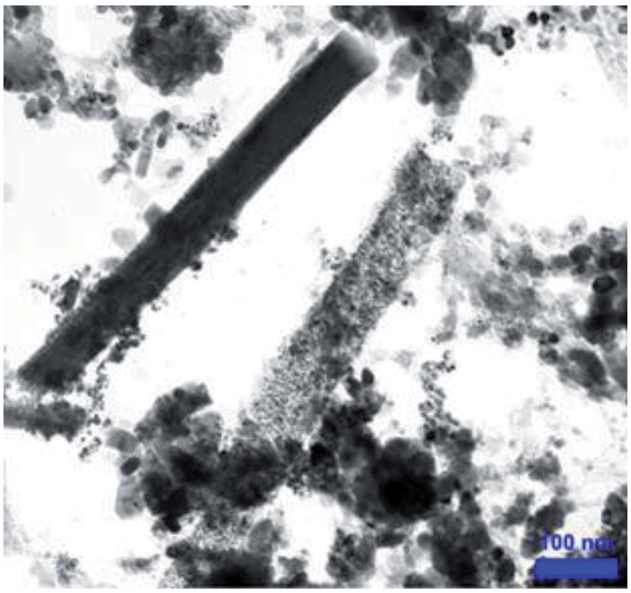

Fig. 5 TEM images of the CFHT nanocomposite.

seen for HNTs,[2–4] the aggregation of the surrounding spherical particles is attributed to modified magnetic iron nanoparticles. The average diameter of the HNTs is about 92 nm in this image. It is noteworthy that the shape of HNTs still has retained after several chemical modifications (Fig. 4).

2.1.5. TEM analysis. As observed in Fig. 5, there are cylindrical like objects with diameters of about 64 nm belonging to HNTs. In addition, a large number of particles with spherical morphologies have been distributed on the surface and between these nanosize HNTs. Attention to detail of the structure of the spherical particles indicated that they are made up of dark-colored cores that can be Fe_3O_4 covered with a lighter shell which can be an organic part of the CFHT nanocomposite. Hence, the functionalization of HNTs was confirmed by this image.

2.1.6. VSM analysis. The magnetic characteristic of the CFHT nanocomposite was studied through VSM analysis at room temperature. The magnetization prepared samples based on the applied magnetic field can be observed in Fig. 6. The remanence (Mr) and coercivity (Hc) constitute are decisive quantities for the classification of magnet materials. When the value of these quantities in VSM analysis is zero, that examined substance is considered as superparamagnetic material. As shown in Fig. 6, when the range of applied magnetic field was about −10 000 to +10 000 oersted, the observed saturation magnetic of the CFHT nanocomposite was approximately 15.88 emu g^{-1}, which decreased compared to the Fe_3O_4@HNTs with 30.62 emu g^{-1} under similar conditions. Since the Fe_3O_4@-HNTs has been modified by several chemical reactions using non-magnetic materials, this decline seems reasonable. The catalyst is sufficiently magnetized to be collected from the reaction mixture by a magnet. But what is the point of a superparamagnetic heterogeneous catalyst being prepared? The striking benefits of utilizing magnetic heterogeneous catalysts in organic reactions include providing a high specific surface area, the ability to be easily separated from the reaction medium and their repeated usability, which is fundamental in terms of time, cost and energy savings at the industrial scale.

2.1.7. TGA analysis. The thermal behavior of the synthesized samples in the final catalyst preparation pathway was performed using TGA analysis and obtained results was illustrated in Fig. 7. In the thermogram of the Fe_3O_4@HNTs–CPTS

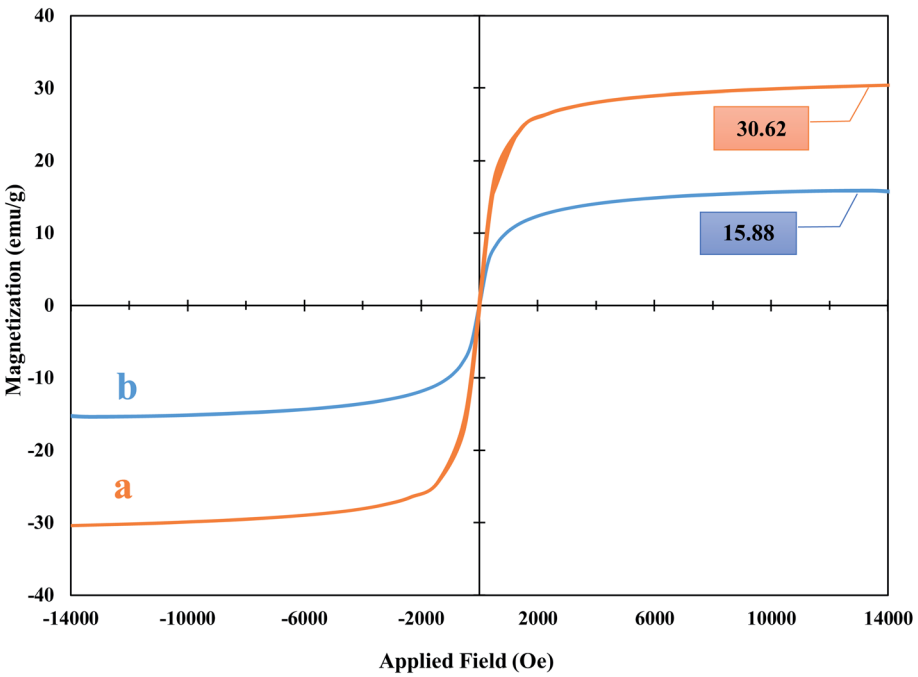

Fig. 6 VSM analysis of Fe_3O_4@HNTs (a) and the CFHT nanocomposite (b).

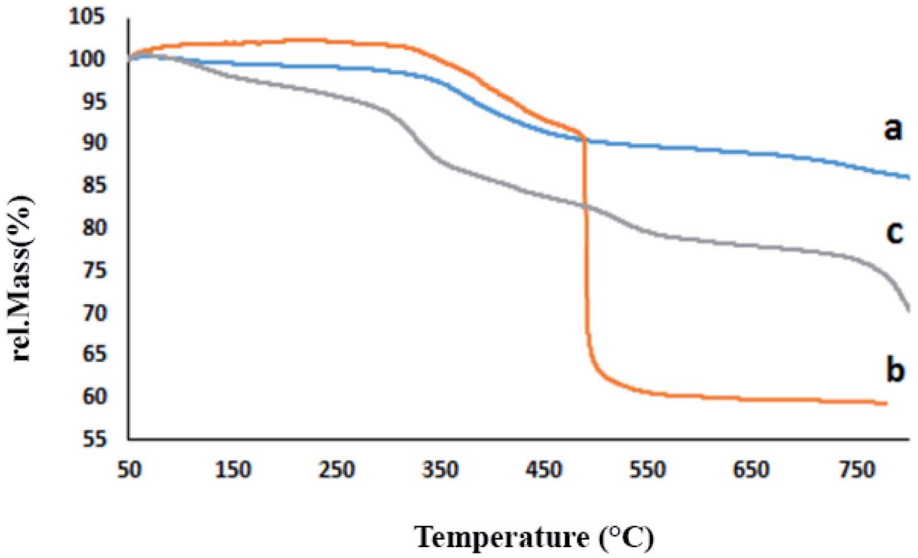

Fig. 7 TGA analysis of the Fe_3O_4@HNTs–CPTS (a), the Fe_3O_4@HNTs–tetrazole (b) and the CFHT nanocomposite (c).

(a), a weight loss less than 5% befallen in the temperature range of 50 to 300 °C related to the volatilization of absorbed solvent on the surface of Fe_3O_4@HNTs–CPTS. The next stage of weight loss in the temperature range 350 to 500 °C is associated to the thermal decomposition of 3-cyanopropyl groups as an organic section.[26] The Fe_3O_4@HNTs–CPTS retains nearly 86% of its weight until 800 °C. In the thermogram of the Fe_3O_4@HNTs–tetrazole (b), appearing weight loss in the temperature range of 50 to 250 °C is attributed with the desorption and removal of solvents. The next weight loss is in the temperature range of 300 to 490 °C, which might be related to the destruction of propyl groups. The severe weight loss appearing in the temperature range of 490 to 550 °C, can be owing to the thermal degradation of the tetrazole ring in addition to the dehydroxylation of Fe_3O_4@HNTs. The residual weight of this material is only about 40% at 800 °C. Comparison of curves (a) and (b) displayed that the click reaction of the Fe_3O_4@HNTs–CPTS with NaN_3 and the fabrication of the tetrazole ring as an organic segment has reduced the thermal resistance of the resulted compound. The CFHT nanocomposite thermogram curve (c) showed that the coordination of Cu(II) on the tetrazole ring of Fe_3O_4@HNTs–tetrazole as an efficient chelating agent, enhanced intensely its thermal stability. Therefore, the CFHT nanocomposite has only a 30% weight loss when the temperature reached to 800 °C.

2.1.8. XRD analysis. As observed in Fig. 8, the XRD analysis of the CFHT nanocomposite was compared with the obtained pattern of F_e3O_4, HNTs, and Cu. The reflection peaks of HNTs at 2θ = 19.99, 35.05 and 26.75° completely compile with the characteristic data of JCPDS card no.00-029-1489. Also, the loading Fe_3O_4 nanoparticles with cubic structure can be confirmed by the diffraction angles (2θ) of 35.84, 42.47, 56.22 and 62.65° according to the JCPDS card number 01-075-0449. Moreover, the Cu crystalline structure was caused to appear the diffraction at 42.47°, 50.61° and 71.99° (JCPDS card no. 00-00-0836).

2.2. Catalytic application of the CFHT nanocomposite in organic synthesis

2.2.1. Optimization of the effective parameters. Investigating the catalytic performance of the fabricated CFHT nanocomposite was done in the synthesis of the 5-substituted 1*H*-tetrazoles derivatives. To determine the optimum condition for the MCRs between aromatic aldehyde (**1**), malononitrile (**2**) and sodium azide (**3**) with the molar ratio of 1 : 1 : 1.2, various solvents, temperature, catalytic quantity were tested. Experimental information on the optimization process has been provided in Table 2. At first, the reaction was carried out under various conditions without catalyst, the data showed that the reaction efficiency was negligible after 100 minutes in all of these experiments. The details of these experiments are presented in Table 2 (data 1 to 2). Therefore, the catalyst has a crucial effect to conduct and boost this reaction. The reaction was then carried out in ethanol and DMF in the presence of different quantities of catalyst. The results showed that 30 mg of catalyst was adequate to conduct the reaction, lower values resulted in reduced efficiency of the reaction. By increasing the catalyst content to 50 mg, not only does not the reaction efficiency improve, but it also decreased slightly. The existence of 30 mg CFHT catalyst in DMF under refluxing conditions was the best condition reaction for the synthesis of the 5-substituted 1*H*-tetrazoles derivatives by MCRs.

Different substituted benzaldehydes with electron drawings and electron-donating groups were tested to evaluate the generality and limitation of this method and some 5-substituted 1*H*-tetrazoles derivatives have made by the Knoevenagel condensation reaction and the 1,3 dipolar cycloaddition reaction of aldehydes (**1**), malononitrile (**2**) and sodium azide (**3**). The nature of substitution on the aromatic aldehydes had no significant difference in the productivity of the related products or the reaction time. Both types of benzaldehydes possessing either electron-withdrawing or electron-donating

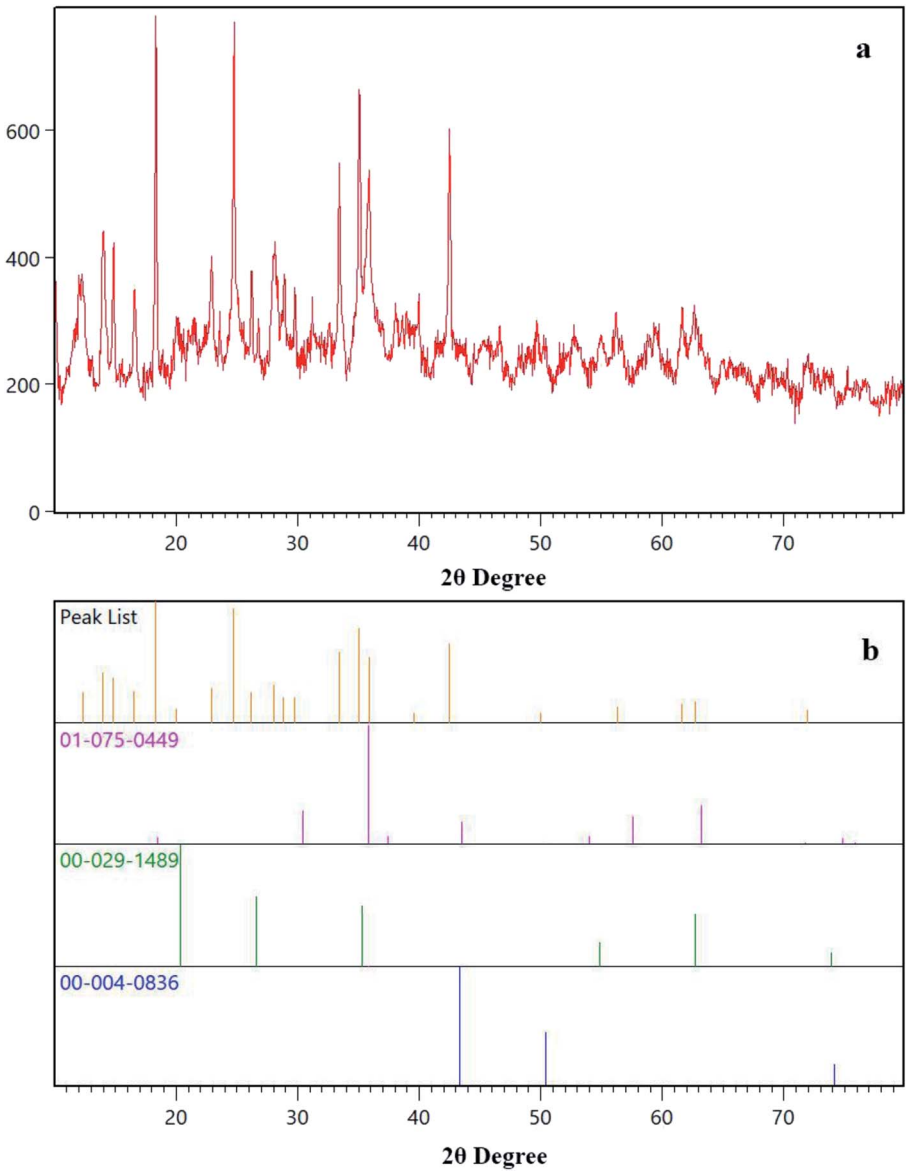

Fig. 8 XRD analysis of the CFHT nanocomposite (a), the Fe_3O_4, HNTs and Cu patterns (b).

Table 2 Optimizing the reaction conditions in the 5-substituted 1*H*-tetrazoles derivatives through MCRs[a]

Entry	Solvent	Amount of catalyst (mg)	Temp. (°C)	Time (min)	Yield[b] (%)
1	Solvent-free	—	r.t.	100	Trace
2	Water	—	r.t.	100	Trace
3	Solvent-free	—	Reflux	100	Trace
4	Ethanol	—	r.t.	100	Trace
5	Ethanol	—	Reflux	100	20
6	Ethanol	30	Reflux	40	38
7	DMF	10	Reflux	40	56
8	DMF	20	Reflux	40	72
9	DMF	30	Reflux	40	97
10	DMF	50	Reflux	40	89

[a] Reaction conditions: aromatic aldehyde (1 mmol), malononitrile (1 mmol) and sodium azide (1.2 mmol), the CFHT nanocatalyst (10–50 mg). [b] The yields relate to the isolated product.

substitutions in the reaction with malononitrile and sodium azide, made desired products with 90–97% efficiency just after 30–40 min (Table 3).

2.3. Recyclability of the CFHT nanocomposite

The superparamagnetic behavior was one of the beneficial features of the constructed nanocomposite which verified by characterization analyzes. This feature, in addition to being a facilitator in the laboratory work due to its simple separation from the reaction mixture, is also important at the industrial application. Furthermore, conducting chemical reactions using retrievable and reusable catalysts is a substantial issue in terms of conserving the environment. In this work, the capacity of the catalyst to be re-used was investigated, in which the catalyst was isolated using magnet after finishing the reaction, washed several times with acetone and dried at room temperature. Then

Table 3 The synthesis of 5-substituted 1*H*-tetrazoles derivatives (**4a–h**) *via* three component reaction using the CFHT nanocatalyst

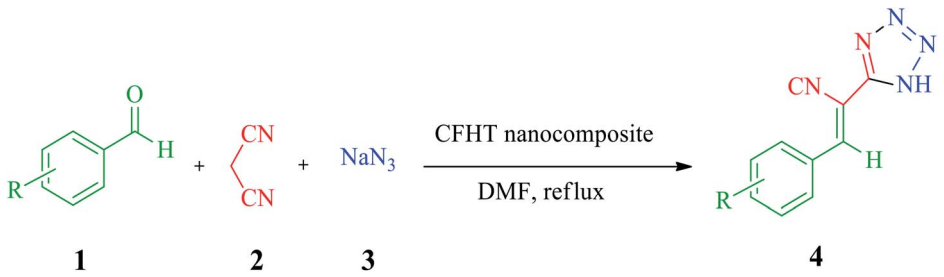

Entry	R	Product	Time (min)	Yield[a] (%)	Mp (°C) Observed	Mp (°C) Literature
1	H	**4a**	40	97	170–171	168–170 (ref. 27)
2	4-NO_2	**4b**	30	93	167–169	166–168 (ref. 27)
3	4-Br	**4c**	40	90	166–168	165–167 (ref. 27)
4	4-OH	**4d**	40	92	160–162	159–161 (ref. 28)
5	4-F	**4e**	30	94	178–179	176–179 (ref. 29)
6	4-OMe	**4f**	40	90	153–154	153–155 (ref. 30)
7	4-Me	**4g**	40	91	190–192	189–191 (ref. 30)
8	3-Me	**4h**	40	95	132–134	130–132 (ref. 30)
9	4-Cl	**4i**	30	92	164–166	165–168 (ref. 29)

[a] The yields relate to the isolated product.

it was reused for five sequential runs in the synthesis of **4a** derivative. As presented in Fig. 9, the reaction efficiency reduced from 97% to 90% after five times of catalyst reuse.

2.4. A mechanism for the synthesis of the 5-substituted 1*H*-tetrazoles derivatives

The suggested mechanism of the synthesis of 5-substituted 1*H*-tetrazoles derivatives is illustrated in Fig. 10. First, the nitrile group of malononitrile and the carbonyl group of aromatic aldehyde were activated by the CFHT nanocatalyst, the Knoevenagel condensation reaction between activated malononitrile and aromatic aldehyde resulted in the formation of arylidenemalononitrile (**I**). Subsequently, by the interaction of Cu from the CFHT nanocatalyst with the N of molecule (**I**), accelerated [3 + 2] cycloaddition reaction between arylidenemalononitrile and sodium azide. Afterward, the catalyst was isolated from a complex (**II**) using acidic conditions workup (aqueous solution of HCl) and the molecule (**III**) was made. Eventually, through the tautomerization of molecule of (**III**), the 5-substituted 1*H*-tetrazoles (**4a–h**) as a more stable tautomer was accomplished.

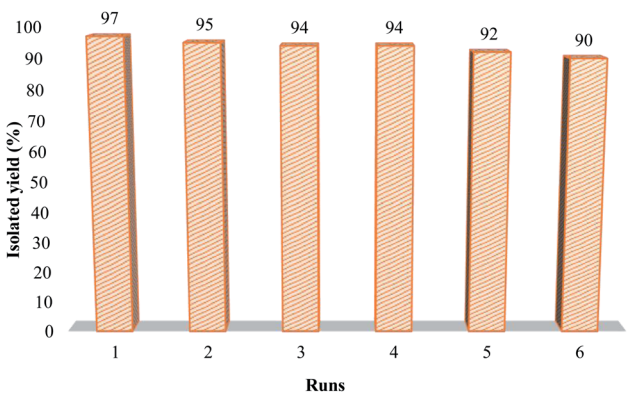

Fig. 9 Recycling diagram of the CFHT nanocatalyst in the synthesis of 4a.

2.5. Antibacterial activity of the CFHT nanocomposite

2.5.1. Agar diffusion assay. The assessment of the antibacterial efficiency of the synthesized CFHT nanocomposite and control samples including Cu(II), 5-substituted 1*H*-tetrazoles, Fe_3O_4@HNTs–CPTS, Fe_3O_4@HNTs–tetrazole against the Gram-negative (*Escherichia coli*) and Gram-positive (*Staphylococcus aureus*) by *in vitro* study and agar diffusion method. The observed zones of inhibition around the examined samples were measured to define their relative antibacterial efficiency against these two types of microorganisms. The growth inhibition zone of all samples against *S. aureus* and *E. coli* were presented in Fig. 11. Also, the details of the inhibition zone width by mentioned samples are listed in Table 4. Although all control samples including Cu(II), 1*H*-tetrazoles, Fe_3O_4@HNTs–CPTS, Fe_3O_4@HNTs–tetrazole exhibited antibacterial efficiency against two bacteria, the CFHT composite demonstrated obviously more antibacterial property than any of control samples in the same conditions. The design of the nanocomposite is such that the simultaneous presence of halloysite, tetrazole, and Cu(II), in its structure has resulted in this noticeable inhibitory effect against studied microorganisms. Furthermore,

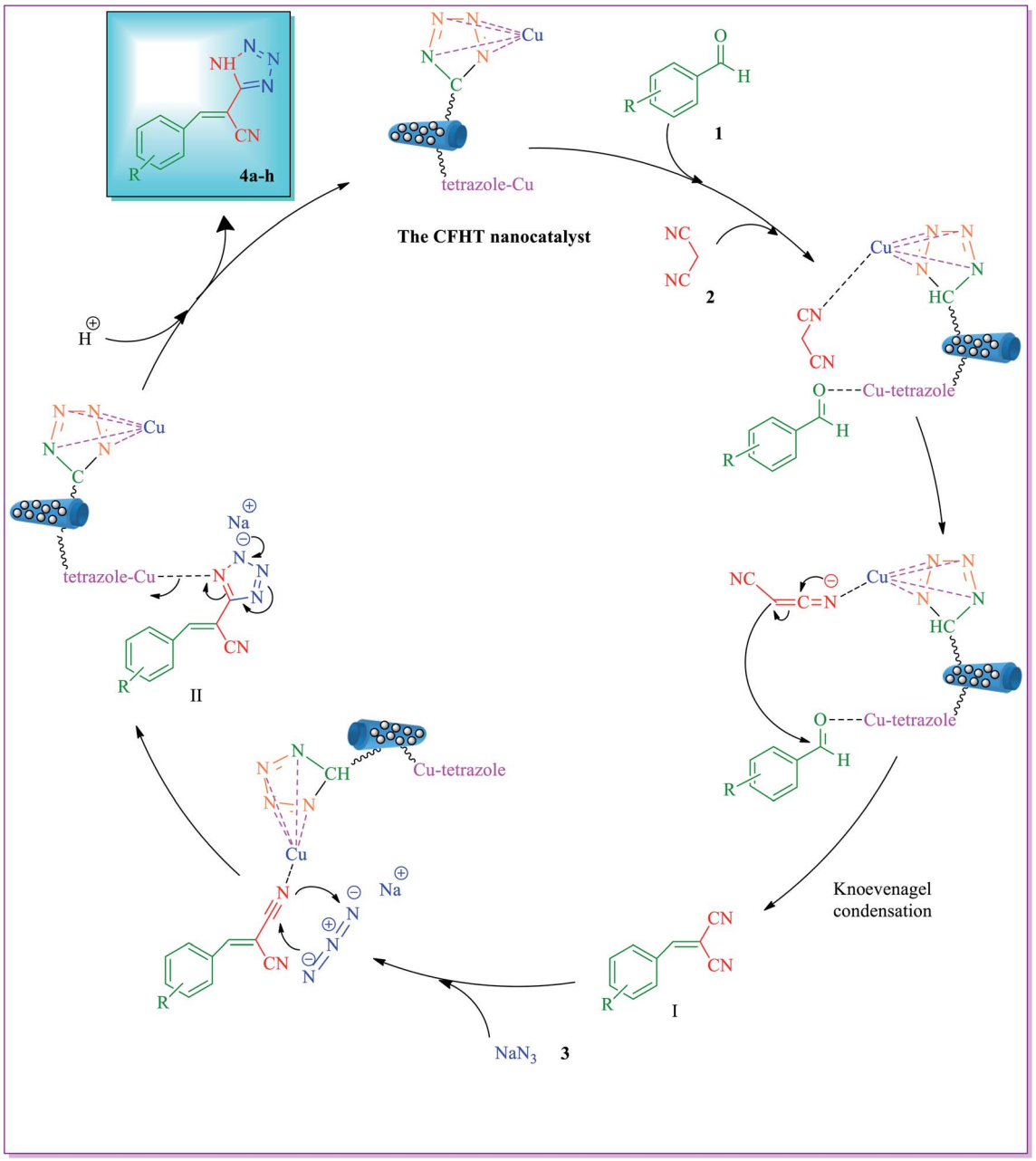

Fig. 10 Suggested mechanism for the synthesis of 5-substituted 1*H*-tetrazoles derivatives (**4a–h**) in the presence of the CFHT nanocatalyst.

a comparison of the obtained result indicates that CFHT nanocomposite exhibited greater antibacterial activity against *S. aureus* as a Gram positive strain than against *E. coli* as a Gram negative strain. The reason for this observation could be related to the difference in the structural features of the studied bacteria cell wall. In Gram-positive bacteria, the cell wall consists of a single layer of peptidoglycan, while the cell wall of Gram-negative bacteria has a relatively complicated structure with two internal and external membranes. The inner membrane is composed of peptidoglycan and the outer membrane is made up of lipoproteins, lipopolysaccharides and phospholipids molecules. This complicated cell wall of Gram-negative bacteria act as a strong barrier to the penetration

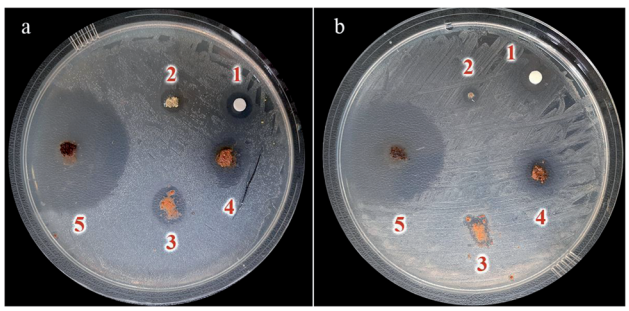

Fig. 11 Inhibition zones of (1) Cu(II), (2) 1*H*-tetrazoles, (3) Fe_3O_4@HNTs–CPTS, (4) Fe_3O_4@HNTs–tetrazole and (5) CFHT nanocomposite against (a) *S. aureus* and (b) *E. coli* bacteria for 24 h.

Table 4 Width of inhibition zones for different samples against *S. aureus* and *E. coli*

Sample	Inhibition zone (diameter), mm *S. aureus*	Inhibition zone (diameter), mm *E. coli*
Cu(II)	3	4
5-Substituted 1*H*-tetrazoles	2	2
Fe_3O_4@HNTs–CPTS	4	3
Fe_3O_4@HNTs–tetrazole	8	7
CFHT nanocomposite	20	16

and entry of a foreign substance into the bacterial cell, thus they are being more resistant than Gram-positive ones.[31]

2.5.2. Plate-count method. The colony plate images of *S. aureus* (ATCC 12600) and *E. coli* (ATCC 9637) bacteria in the presence of various nanocomposite (Fe_3O_4@HNTs–CPTS, Fe_3O_4@HNTs–tetrazole, and CFHT) are observed in Fig. 12. As the results of these experiments, the high number of *E. coli* and *S. aureus* were killed by treatment with the CFHT nanocomposite compare to the control of *E. coli* and *S. aureus* microorganisms. The reduction of both bacteria was not significant by Fe_3O_4@HNTs–CPTS, and Fe_3O_4@HNTs–tetrazole nanocomposite. The comparison of images of (a) and (b) indicated that this reduction in number of *S. aureus* colonies were considerably higher than in *E. coli.* The difference in the cell wall structure of these two types of bacteria may have caused this observation.

3. Experimental

3.1. General

All consumed chemicals, reagents and solvents were bought from Sigma Aldrich and Merck companies. Monitoring the progress of catalytic reactions was done by thin-layer chromatography (TLC). Melting points of all synthesized derivatives were measured with an Electrothermal 9100 apparatus. FT-IR spectra were recorded on a Shimadzu IR-470 spectrometer in the range of 400 to 4000 cm^{-1} by KBr pellets. ^1H and ^{13}C NMR spectra were recorded on a Bruker DRX-500 spectrometer at 500 and 125 MHz, respectively. Elemental analysis of prepared samples was performed by EDX analysis recorded on Numerix JEOL-JDX 8030 (30 kV, 20 mA). The XRD pattern of the fabricated composites were obtained by Bruker D8 Advance X-ray diffractometer. The morphology and structure of the nanocatalyst were studied by SEM, VEGA2 TESCAN instrument. TEM image was achieved by a Philips CM120 instrument. The magnetic properties of the prepared samples were identified at room temperature using VSM analysis, accomplished by LBKFB model-magnetic Kashan Kavir, thermogravimetric analysis (TGA) was performed using a Bahr-STA 504 instrument, and Eager 300 for EA1112 was used for CHNS analysis.

3.2. Catalyst synthesis pathway

As mentioned, the synthesis of CFHT nanocomposite was performed by some following steps.

3.2.1. The preparation of Fe_3O_4@HNTs. 0.3 g $FeCl_3 \cdot 6H_2O$ (1.85 mmol) and 0.2 g $FeCl_2 \cdot 4H_2O$ (1 mmol) added to a round bottom flask containing 2 g sonicated HNTs in 10 mL of distilled water at room temperature under magnetic stirring. The temperature of the mixture gradually increased to 80 °C. In the second step, the addition of NH_4OH (25%) solution to extremely stirring mixture afforded alkaline condition to generate a magnetic HNTs. The appearance of the mixture changed to black suspension signifying the MNPs formation in the presence of HNTs as natural support. The stirring of mixture was continued for 45 min at 80 °C. The resulting precipitate was collected by a magnet, washed with distilled water and ethanol for removing probable unreacted salts and reagent, then dried in an oven at 80 °C for about 4 h to get Fe_3O_4@HNTs.

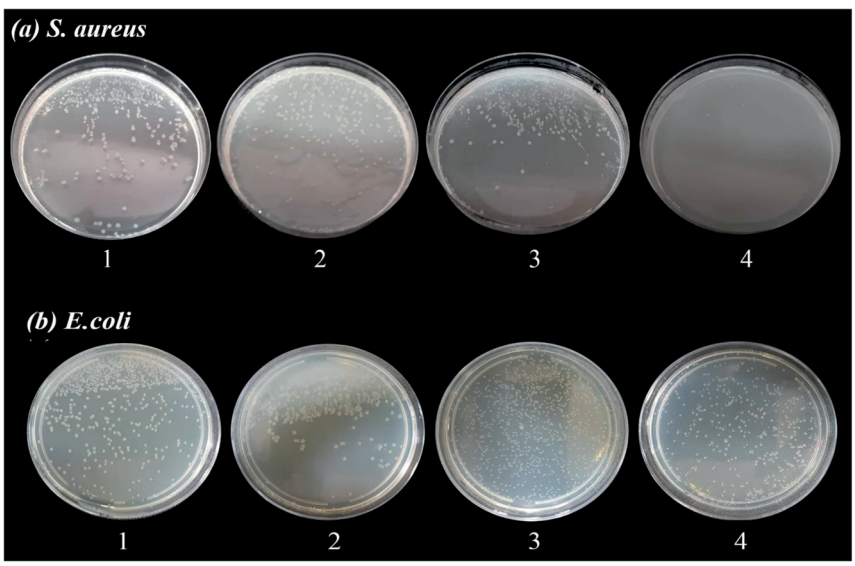

Fig. 12 Colony counter images of *S. aureus* (a) and *E. coli* (b) after 24 h of incubation, (1) before treatment (control plate), after treatment with (2) Fe_3O_4@HNTs–CPTS, (3) Fe_3O_4@HNTs–tetrazole, and (4) synthesized CFHT nanocomposite.

3.2.2. The synthesis of Fe_3O_4@HNTs–CPTMS. For modification of Fe_3O_4@HNTs, 2 g magnetic HNTs were stirred in 17 mL toluene under N_2 atmosphere for about 30 min in a round bottom flask, then 2 mL CPTMS added stirring magnetic HNTs, the reaction was kept on two days under refluxing condition. The crude precipitate effortlessly collected by magnetic force, washed several times by ethanol to obtain Fe_3O_4@HNTs–CPTMS and dried in an oven at 80 °C for 4 h.

3.2.3. The synthesis of Fe_3O_4@HNTs–CPTS. 3 g KI added to 2 g Fe_3O_4@HNTs–CPTMS in 15 mL acetonitrile, then the mixture was stirred for about 30 min at room temperature, then NaCN (3.4 g) was added to above mixture and reaction was kept on stirring under refluxing condition for 48 h to achieve the Fe_3O_4@HNTs–CPTS nanocomposite. And the end, the fabricated material was collected, washed with deionized water and dried in an oven at 60 °C for 6 h.

3.2.4. The preparation of Fe_3O_4@HNTs–tetrazole and CFHT nanocomposite. After several step modifications of the Fe_3O_4@HNTs, 3.5 g NaN_3 and 3 g Fe_3O_4@HNTs–CPTS in DMF were refluxed for 48 h. The reaction [3 + 2] cycloaddition reaction between Fe_3O_4@HNTs–CPTS and NaN_3 resulted in the generation of tetrazole rings. The product of this stage was isolated by a magnet, washed with water several times and dried in an oven at 60 °C. The final stage was Cu(II) loading onto the Fe_3O_4@HNTs–tetrazole by using 4 g of $Cu(SO_4)_2$ in 50 mL of distilled water for 12 h to obtain the CFHT nanocomposite.

3.3. A typical procedure for the preparation of the 5-substituted 1*H*-tetrazoles derivatives

CFHT nanocatalyst (0.03 g), aromatic aldehyde (1.00 mmol), malononitrile (1.00 mmol), and NaN_3 (1.20 mmol) were mixed and stirred in 5 mL DMF, then the mixture was refluxed. The reaction development was checked by TLC (*n*-hexane–ethyl acetate, 2 : 1), after completion of the reaction, the reaction mixture was filtered. Then, to get the precipitate of the product, a 20 mL aqueous solution of HCl (2 M) was poured to the filtrate under extreme stirring. The obtained precipitate was again filtered and dried in an oven to provide the 5-substituted 1*H*-tetrazoles derivatives. Spectral and analytical analyses structures of some synthesized products confirmed their structures.

3.3.1. Spectral data of the selected products. 3-(4-Chlorophenyl)-2-(1*H*-tetrazol-5-yl)acrylonitrile (**4i**): ^{1}H-NMR (500 MHz, DMSO): δ_H (ppm) = 3.40 (1H, s, NH), 7.68 (2H, dd, J = 8 Hz, H–Ar), 8.03 (2H, dd, J = 8 Hz, H–Ar), 8.45 (1H, s, CH); ^{13}C NMR (125 MHz, DMSO); δ_C (ppm) = 109.6, 119.9, 129.5, 131.6, 135.1, 136.9, 146.7, 155.1.

3.4. Procedure for antibacterial studies

Evaluation of the antibacterial activity of the prepared samples was carried out through using the standard agar diffusion and the colony counter methods against *E. coli* as a Gram-negative (ATCC 9637) and *S. aureus* as a Gram-positive (ATCC 12600) bacteria. All the instruments and glassware were sterilized at 121 °C for 10 min in an autoclave before each examination. Agar was employed as a base medium and a solid growth medium plus nutrients microorganisms. Firstly, for disk diffusion tests, the suspensions with 0.5 McFarland turbidity of *S. aureus* and *E. coli* were prepared. Then the 0.01 g of samples (Fe_3O_4@HNTs–CPTS, Fe_3O_4@HNTs–tetrazole, and CFHT nanocomposite), 0.001 g of 1*H*-tetrazole and Cu(II) filter paper disc were added to Muller-Hinton agar culture medium containing bacteria, separately. The results of their antibacterial properties were checked by keeping the Petri dishes at 37 °C in an incubator for 24 h. To assess the relative antibacterial effects of the nanocomposite against two kinds of bacteria, the inhibition zones around the disk were measured. Next, for the colony counter method, at first *S. aureus* and *E. coli* 0.5 McFarland turbidity standard was added to 0.2 mL DMSO and a 0.1 g of the samples. The samples were stirred for 1 h and the following, 0.01 mL of the solution was added to Mueller Hinton agar media. The dishes were kept at 37 °C for 24 h for growing bacteria and form different colonies.

4. Conclusion

The CFHT nanocomposite was prepared based on HNTs as a naturally occurring mesoporous material, inexpensive and readily available salts and reagents through several chemical reactions. The conventional analyses identified the nanocomposites and confirmed the fabrication of the CFHT nanocomposite. The VSM analysis shows that the magnetic saturation of the final nanocomposite is adequate to be easily separated from the reaction medium which can be beneficial to save time, cost and energy at the industrial scale. Thermogravimetric study investigations have revealed that although by the formation of tetrazole on the surface of the magnetic HNTs, the thermal resistance decreases, this is well compensated by the coordination of the Cu(II) on the tetrazole rings. The CFHT nanocomposite retains about 70% of its weight up to 800 °C. The SEM and TEM images of this nanocomposite demonstrated that the morphology of the HNTs has not changed over some modification reactions to generate the desired functional groups. Evaluation of catalytic performance of the prepared nanocomposite in the synthesis of 5-substituted 1*H*-tetrazoles derivatives showed that it was an effectives catalyst for obtaining desired products with high yield (90–97%) in short reaction time (30–40 min). According to the presented suggested mechanism, the prepared nanocomposite played a vital role in both the Knoevenagel condensation and [3 + 2] cycloaddition reaction. Furthermore, the zone of inhibition around 16 and 20 mm for *E. coli* and *S. aureus* bacteria revealed the considerable antibacterial efficacy of CFHT nanocomposite.

Conflicts of interest

The authors declare no conflict of interest.

Acknowledgements

All authors gratefully acknowledge the partial support from the Research Council of the Iran University of Science and Technology (IUST).

References

1 S. Barrientos-Ramírez, G. M. de Oca-Ramírez, E. Ramos-Fernández, A. Sepúlveda-Escribano, M. Pastor-Blas and A. González-Montiel, *Appl. Catal., A*, 2011, **406**, 22–33.
2 S. Hillier, R. Brydson, E. Delbos, T. Fraser, N. Gray, H. Pendlowski, I. Phillips, J. Robertson and I. Wilson, *Clay Miner.*, 2016, **51**, 325–350.
3 Z. Hajizadeh and A. Maleki, *Mol. Catal.*, 2018, **460**, 87–93.
4 D. Rawtani and Y. K. Agrawal, *Rev. Adv. Mater. Sci.*, 2012, **30**, 282–295.
5 Z. Hajizadeh, K. Valadi, R. Taheri-Ledari and A. Maleki, *ChemistrySelect*, 2020, **5**, 2441–2448.
6 Y. M. Lvov, D. G. Shchukin, H. Mohwald and R. R. Price, *ACS Nano*, 2008, **2**, 814–820.
7 R. F. Fakhrullin and Y. M. Lvov, *Nanomedicine*, 2016, **11**, 2243–2246.
8 A. Maleki, Z. Hajizadeh and P. Salehi, *Sci. Rep.*, 2019, **9**, 1–8.
9 A. Maleki, Z. Hajizadeh and R. Firouzi-Haji, *Microporous Mesoporous Mater.*, 2018, **259**, 46–53.
10 A. Maleki and Z. Hajizadeh, *Silicon*, 2019, **11**, 2789–2798.
11 D. Marković, C. Deeks, T. Nunney, Ž. Radovanović, M. Radoičić, Z. Šaponjić and M. Radetić, *Carbohydr. Polym.*, 2018, **200**, 173–182.
12 A. H. Gemeay, M. E. El-Halwagy, R. G. El-Sharkawy and A. B. Zaki, *J. Environ. Chem. Eng.*, 2017, **5**, 2761–2772.
13 W. Yuan, C. Zhang, H. Wei, Q. Wang and K. Li, *RSC Adv.*, 2017, **7**, 22825–22835.
14 A. Zarnegaryan, M. Moghadam, S. Tangestaninejad, V. Mirkhani and I. Mohammdpoor-Baltork, *New J. Chem.*, 2016, **40**, 2280–2286.
15 M. Rezaei, K. Amani and K. Darvishi, *Catal. Commun.*, 2017, **91**, 38–42.
16 D. Solairaj, P. Rameshthangam, P. Muthukumaran and J. Wilson, *Int. J. Biol. Macromol.*, 2017, **101**, 668–679.
17 M. Zhang, Y. H. Liu, Z. R. Shang, H. C. Hu and Z. H. Zhang, *Catal. Commun.*, 2017, **88**, 39–44.
18 M. A. Maleki, Z. Hajizadeh and H. Abbasi, *Carbon Lett.*, 2018, **27**, 42–49.
19 A. Domling, W. Wang and K. Wang, *Chem. Rev.*, 2012, **112**, 3083–3135.
20 A. Maleki, F. Hassanzadeh-Afruzi, Z. Varzi and M. S. Esmaeili, *Mater. Sci. Eng., C*, 2020, **109**, 110502.
21 A. Maleki, Z. Varzi and F. Hassanzadeh-Afruzi, *Polyhedron*, 2019, **171**, 193–202.
22 C. G. Neochoritis, T. Zhao and A. Dömling, *Chem. Rev.*, 2019, **119**, 1970–2042.
23 M. Esmaeilpour, A. R. Sardarian and H. Firouzabadi, *Appl. Organomet. Chem.*, 2018, **32**, e4300.
24 T. Jin, F. Kitahara, S. Kamijo and Y. Yamamoto, *Chem.–Asian J.*, 2008, **3**, 1575–1580.
25 N. Ahmed and Z. N. Siddiqui, *RSC Adv.*, 2015, **5**, 16707–16717.
26 M. Jafarzadeh, E. Soleimani, P. Norouzi, R. Adnan and H. Sepahvand, *J. Fluorine Chem.*, 2015, **178**, 219–224.
27 Z. N. Tisseh, M. Dabiri, M. Nobahar, H. R. Khavasi and A. Bazgir, *Tetrahedron*, 2012, **68**, 1769–1773.
28 M. Bakherad, R. Doosti, A. Keivanloo, M. Gholizadeh and K. Jadidi, *J. Iran. Chem. Soc.*, 2017, **14**, 2591–2597.
29 P. Akbarzadeh, N. Koukabi and E. Kolvari, *Res. Chem. Intermed.*, 2019, **45**, 1009–1024.
30 J. Safaei-Ghomi and S. Paymard-Samani, *Chem. Heterocycl. Compd.*, 2015, **50**, 1567–1574.
31 A. S. Kritchenkov, A. R. Egorov, I. S. Krytchankou, N. V. Dubashynskaya, O. V. Volkova, T. V. Shakola and Y. A. Skorik, *Int. J. Biol. Macromol.*, 2019, **132**, 340–350.